Ionics (2021) 27:1977–1986
https://doi.org/10.1007/s11581-021-03936-y

ORIGINAL PAPER

# Unique three-dimensional hierarchical heterogeneous $MoS_2$/graphene structures as a high-performance anode material for lithium-ion batteries

Fei Long[1,2] · Yi Chen[1] · Caihong Wu[1] · Jilin Wang[1,3] · Shuyi Mo[2,3] · Zhengguang Zou[1,2] · Guoyuan Zheng[1,2]

Received: 31 December 2020 / Revised: 27 January 2021 / Accepted: 28 January 2021 / Published online: 12 March 2021
© The Author(s), under exclusive licence to Springer-Verlag GmbH Germany, part of Springer Nature 2021

## Abstract

A unique $MoS_2$/graphene composite ($MoS_2$/GrF) was synthesized via a facile hydrothermal method. XRD, FESEM, EDS, TEM, HRTEM, XPS, and BET analyses were performed to characterize the as-synthesized samples. The samples were demonstrated to present interesting uniform three-dimensional hierarchical heterogeneous structures where $MoS_2$ microspheres (with an average diameter of 750 nm) penetrated the graphene layer. By the "space-confined" effect, the (002) plane of $MoS_2$ is inhibited when grown in the interlayer of GO, which increases the interlayer spacing and improves the rate performance of the electrode. Moreover, $MoS_2$ that grows between the graphene layers can form a good contact, reducing the contact resistance. As an anode material for lithium-ion batteries, the $MoS_2$/GrF electrode exhibited an outstanding reversible capacity (1510 mAh $g^{-1}$ at 100 mA $g^{-1}$ after 200 cycles) and excellent rate performance (~990 mAh $g^{-1}$ at 1000 mA $g^{-1}$).

**Keywords** Molybdenum disulfide · Graphene · Space-confined · Rate performance · Li-ion batteries

## Introduction

Lithium-ion batteries (LIBs) [1], potassium-ion batteries (KIBs) [2], and sodium ion batteries (SIBs) [3–5] are the research hotspots in the field of energy storage. Among them, LIBs are considered the leading energy storage device for electric vehicles because of their high energy density, long cycle, and environmental friendliness properties. As a major part of LIBs, the anode material could determine the cost, performance, safety, and life of LIBs. The current commercialized anode material is graphite. However, graphite cannot meet the increasing demands on LIBs due to its low theoretical capacity (372 mAh $g^{-1}$) and barely passable rate capability performance [1, 6]. Molybdenum disulfide ($MoS_2$) is considered the best alternative to graphene because of its high theoretical capacity (~670 mAh $g^{-1}$) [7]. However, $MoS_2$ has many disadvantages as electrode material. On the one hand, the crystal structure will be destroyed in the process of lithiation and delithiation, because of the weak interlaminar van der Waals force of $MoS_2$. On the other hand, the conductivity of $MoS_2$ is low, which leads to poor rate performance [8]. In addition, the lithium product $Li_2S$ reacts with the electrolyte to form a thick gel polymer layer to resist the ion channel. Therefore, nanostructure and enhanced conductivity are main methods to improve the electrochemical performance of $MoS_2$. Recently, researchers found that combining $MoS_2$ with carbon-based materials could enhance the electronic conductivity while concurrently buffering the volume changes in $MoS_2$ during the charge/discharge process, ultimately providing fast electrode kinetics and stable cycling performance [9, 10]. There are many types of carbon-based materials, such as amorphous carbon [6], carbon fibers [11], porous carbon [12], carbon spheres [13], carbon nanotubes [14, 15],, and graphene [16–19]. Among these carbonaceous materials, graphene has attracted a considerable amount of attention due to its high electrical conductivity, excellent mechanical properties, and large specific surface area. Therefore, $MoS_2$/graphene ($MoS_2$/G) showed a higher specific capacity

✉ Guoyuan Zheng
zhengguoyuan@glut.edu.cn

[1] School of Materials Science and Engineering, Guangxi Key Laboratory of Optical and Electronic Materials and Devices, Guilin University of Technology, Guilin 541004, China

[2] Key Laboratory of New Processing Technology for Nonferrous Metals and Materials, Ministry of Education, Guilin 541004, China

[3] Collaborative Innovation Center for Exploration of Nonferrous Metal Deposits and Efficient Utilization of Resources, Guilin University of Technology, Guilin 541004, China

and more stable circulation performance than other carbon-based materials. In addition, the different morphologies of $MoS_2$/G also presented high capacities, such as three-dimensional porous [20], honeycomb [21],, and nanosheets [22]. Teng et al. [23] designed a kind of $MoS_2$/Gr composite in which $MoS_2$ grew vertically on graphene. This unique structure provided abundant reactive sites and greatly shortened the diffusion distance of $Li^+$. Moreover, the formation of C-O-Mo bond between $MoS_2$ and graphene could enhance the electron transport rate and structural stability. As a result, the $MoS_2$/Gr electrode exhibited an outstanding reversible capacity of 1077 mAh $g^{-1}$ at 100 mA $g^{-1}$ and an excellent cycling performance of 907 mAh $g^{-1}$ at 1000 mA $g^{-1}$ for 400 cycles. Shan et al. [24] prepared N-doped graphene and ultrathin honeycomb-like $MoS_2$ nanosheets, and the resulting composite displayed a unique hierarchical film-foam-film (3F) top-down architecture. The special structure demonstrated an ultrahigh discharge capacity of 1875 mAh $g^{-1}$ at 100 mA $g^{-1}$, an excellent rate capability of 700 mAh $g^{-1}$ at 5.0 A $g^{-1}$, and a long lifetime of 400 cycles with 980 mAh $g^{-1}$ retained.

Herein, we demonstrate a facile approach to prepare an interesting $MoS_2$/graphene hierarchical nanostructure (called "$MoS_2$/GrF") by a hydrothermal process, utilizing the "space-confined" effect of GO. The so-called space-confined is used for layered materials or porous structures such as LDHs, graphene, and fullerene to achieve the purpose of limiting the growth size of nanomaterials. X-ray diffraction (XRD), field-emission scanning electron microscopy (FESEM), transmission electron microscopy (TEM), high-resolution TEM (HRTEM), and X-ray photoelectron spectroscopy (XPS) analyses were carried out to characterize the phase and morphology and bond characteristics. Based on the experimental results, the possible reaction during the preparation of the unique $MoS_2$/graphene three-dimensional hierarchical heterogeneous structures and the likely corresponding growth mechanism were discussed. Finally, a $MoS_2$/GrF electrode yielded an outstanding reversible capacity of 1510 mAh $g^{-1}$ at 100 mA $g^{-1}$ after 200 cycles and an excellent rate performance of ~990 mAh $g^{-1}$ at 1000 mA $g^{-1}$. The key influencing factors in the outstanding performance of the $MoS_2$/GrF electrode, such as structural stability, microstructure, and bond characteristics, were also investigated.

## Experimental section

### Synthesis of graphene oxide

Graphene oxide (GO) was synthesized by the chemical oxidation of natural graphite powder (98.5%) by a modified Hummers method [25], and the detailed preparation process of GO can be seen in the supporting information.

### Synthesis of the unique hierarchical structure of $MoS_2$/GrF

First, 1 g of GO solution was added to 60 mL of deionized (DI) water (Milli-Q, 18.2 MΩ) and stirred for 30 min at room temperature. Then, 0.309 g of ammonium molybdate tetrahydrate ($(NH4)_6Mo_7O_{24}{\cdot}4H_2O$, 99%) powder was added to the mixture and stirred for 30 min. Next, 1 M/L NaOH was added into the mixture until the pH reached 10, and 0.533 g of thiourea ($CH_4N_2S$, 99%) was added to the solution and stirred for 30 min. Finally, the mixture solution was transferred into a 100 mL Teflon-lined stainless steel autoclave, sealed and heated at 200 °C for 24 h. After cooling naturally, the black precipitates were collected by centrifugation, washed with DI water and ethanol several times, and dried by vacuum freezing for 24 h. Finally, $MoS_2$/GrF composites were prepared after the black precipitates were annealed in a conventional tube furnace at 800 °C for 2 h in a nitrogen environment.

The preparation process of $MoS_2$/Gr is similar to that of $MoS_2$/GrF, except that GO requires ultrasonic pretreatment for 1 h.

### Characterization

The X-ray diffraction (XRD) patterns were obtained on an X-ray diffractometer (PANalytical) equipped with a rotating anode using Cu K$\alpha$ as a radiation source ($\lambda$=0.15406 nm). Field-emission scanning electron microscopy (FESEM) images were acquired with a field-emission scanning electron microscope (S-4800). Transmission electron microscopy (TEM) and high-resolution TEM (HRTEM) images were recorded on a JEM-2100F microscope operating at 200 kV. X-ray photoelectron spectroscopy (XPS) spectra were collected on an ESCALAB 250Xi XPS spectrometer. The specific surface area was measured on a NOVA-1200e analyzer at −196 °C.

### Electrochemical measurements

Two-electrode test cells were used for the electrochemical measurements. The working electrodes were fabricated by mixing 80 wt% of active material ($MoS_2$, $MoS_2$/G, or $MoS_2$/GrF), 10 wt% of acetylene black as a conducting agent, and 10 wt% of binder (polyvinylidene fluoride) in N-methyl-2-pyrrolidinone (NMP) on a copper foil. The obtained slurries were then spread uniformly on the copper foil. The coated electrode was dried at 120 °C under vacuum for 12 h and then compressed. Electrochemical measurements were performed using coin cells (CR2025) with Li foil as the counter electrode and microporous membrane (Celgard) as the separator. The electrolyte solution was 1 M $LiPF_6$ dissolved in a mixture of ethylene carbonate, dimethyl carbonate, and ethyl methyl carbonate with a volume ratio of 1:1:1. Galvanostatic charge/discharge cycles were carried out on a CT-3008 (Neware

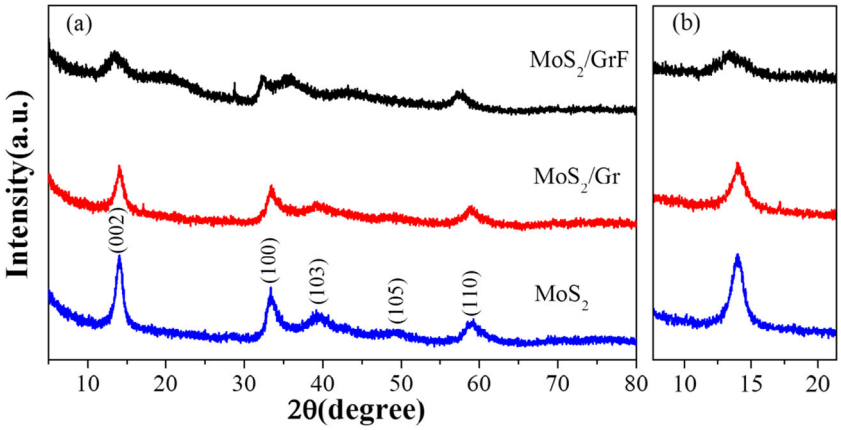


**Fig. 1** XRD patterns of **a** $MoS_2$, $MoS_2$/Gr, and $MoS_2$/GrF prepared by the hydrothermal route and an annealing process performed in $N_2$ at 800 °C for 2 h and **b** an enlarged view of the low-angle region

Shenzhen) battery tester between 0.01 and 3.00 V at various current densities. Cyclic voltammetry (CV) measurements and electrochemical impedance spectroscopy (EIS) tests were performed on an electrochemical workstation (CHI 660E Shanghai) with a potential range of 0.01–3.0 V vs. $Li/Li^+$ at a scan rate of 0.5 mV $s^{-1}$ by applying a sine wave with an amplitude of 0.5 mV in the frequency range of 200–0.01 Hz.

## Results and discussion

Figure 1 shows the XRD patterns of the $MoS_2$, $MoS_2$/Gr, and $MoS_2$/GrF samples prepared by the hydrothermal route and an annealing process performed in $N_2$ at 800 °C for 2 h. As shown in Fig. 1a, the diffraction peaks of all samples can be ascribed to the hexagonal $MoS_2$ phase (JCPDS card number 75-1539) without any other visible phase. Furthermore, the peak attributed to the (002) plane of restacked reduced graphene oxide (rGO) cannot be found in the $MoS_2$/Gr and $MoS_2$/GrF spectra, implying a high dispersion state of rGO in the samples [26]. In addition, among the samples, the $MoS_2$/GrF sample exhibited the weakest diffraction peaks attributed to the (002) plane of $MoS_2$. This finding indicated that the restacking of $MoS_2$ layers can be limited in the $MoS_2$/GrF sample. The diffraction patterns of the three samples at $2\theta$=7~22° are illustrated in Fig. 1b. Comparing the three samples reveals the (002) plane of $MoS_2$/GrF is located at a lower degree than those of the other samples, indicating that the lattice plane spacing corresponding to the (002) plane of $MoS_2$/GrF is larger than that of $MoS_2$ and $MoS_2$/Gr.

Figure 2 shows typical FESEM images of the pure $MoS_2$ (a, b), $MoS_2$/Gr (c, d), and $MoS_2$/GrF (e, f) samples. As shown in Fig. 2a and b, many $MoS_2$ microspheres were distributed homogeneously. Moreover, each $MoS_2$ microsphere, which has

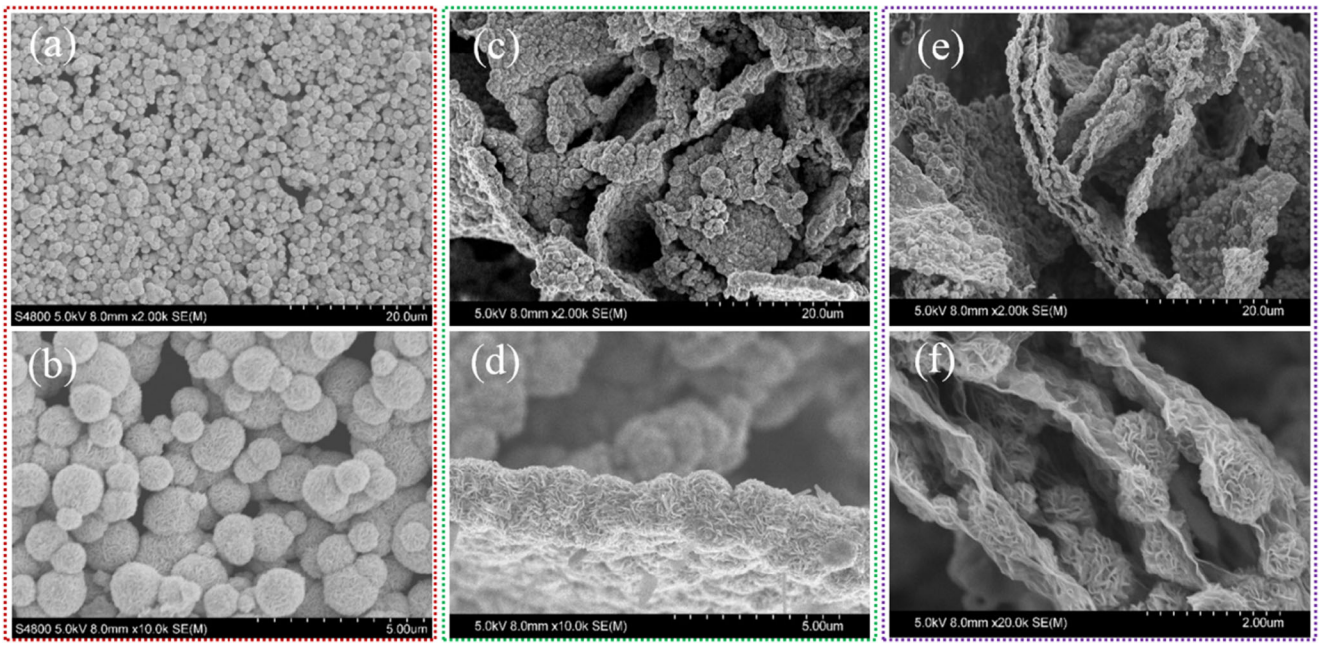


**Fig. 2** FESEM images of a, b $MoS_2$, c, d $MoS_2$/Gr, and e, f $MoS_2$/GrF samples

**Table 1** The elemental content of different samples

| Sample | Element | | | |
|---|---|---|---|---|
| | C | O | S | Mo |
| $MoS_2$ | – | 0.65 | 65.94 | 33.41 |
| $MoS_2$/Gr | 39.43 | 4.89 | 36.73 | 18.95 |
| $MoS_2$/GrF | 42.65 | 6.55 | 33.01 | 17.79 |

an average diameter of approximately 1.5 μm, was formed by the assembly of a large number of nanosheets. This result demonstrated that a flower-like structure of $MoS_2$ can be obtained in an alkaline solution at pH ~10. The $MoS_2$/Gr sample is shown in Fig. 2c and d. Many $MoS_2$ flower-like nanoparticles assembled along the plane direction and formed a sheet with a thickness of approximately 1.5 μm. In addition, it was strange that graphene nanosheets were not observed. However, the EDS results demonstrated the existence of carbon in the $MoS_2$/Gr samples (Table 1; the samples are pressed into a 5-mm diameter wafer), implying that the $MoS_2$ nanosheets grew in situ on graphene and covered all of the graphene surfaces. The $MoS_2$/GrF sample is shown in Fig. 2e and f, which shows that the flower-like $MoS_2$ nanosheets were dispersed on the graphene surface and interlayer. The diameter of the $MoS_2$ microspheres was in the range of 500–700 nm. Compared with $MoS_2$/Gr, $MoS_2$/GrF presented a unique three-dimensional hierarchical heterogeneous structure, suggesting that the ultrasonic treatment of the GO solution before the hydrothermal procedure had an important influence on the structure of the samples. In fact, Fig. 2f shows that many flower-like $MoS_2$ spheres passed across the graphene.

The microstructures of the samples were investigated through TEM (Fig. 3a–c) and HRTEM (Fig. 3d–f). The $MoS_2$ samples displayed flower-like spherical structures with diameters of 1–1.2 μm, and these spherical structures were formed by the self-assembly of many $MoS_2$ nanosheets (Fig. 3a). The corresponding HRTEM image (Fig. 3d) revealed that $MoS_2$ nanoflakes were stacked to form structures with more than 13 layers and that the average lattice plane spacing was approximately 0.62 nm. As shown in Fig. 3b, $MoS_2$/Gr also presented obvious flower-like spherical morphology ($MoS_2$), which grew on the surface of the graphene sheets. In addition, the lattice plane spacings of the nanoflakes (Fig. 3e) were approximately 0.64 nm, which corresponded to the (002) crystal plane of $MoS_2$ and structures comprising approximately 8 stacked layers. For the $MoS_2$/GrF (Fig. 3c), the flower-like spherical morphology of $MoS_2$ grown in situ on graphene did not completely cover the surface of graphene. Interestingly, as labeled in the HRTEM images (Fig. 3f), the lattice plane spacing (0.72 nm) corresponded to the (002) plane of $MoS_2$ and was larger than those of pure $MoS_2$ (Fig. 3d, 0.62 nm) and $MoS_2$/Gr (Fig. 3e, 0.64 nm). The HRTEM results were consistent with those from the abovementioned XRD patterns. In addition, comparing the structures in Fig. 3d–f, it is clearly seen that the $MoS_2$ nanoflakes of $MoS_2$/GrF were stacked to form structures with 5~6 layers, which were fewer than those of $MoS_2$/Gr (8~10 layers) and $MoS_2$ (13~15 layers). This result proved that the (002) plane of $MoS_2$ can be inhibited by the growth of a GO interlayer. Thus, fewer crystal layers will lead to weak van der Waals forces and increase the lattice plane spacing. This expanded lattice plane spacing of the (002) plane of $MoS_2$ could significantly improve the lithium storage capacity and rate capability of $MoS_2$ electrodes [27, 28].

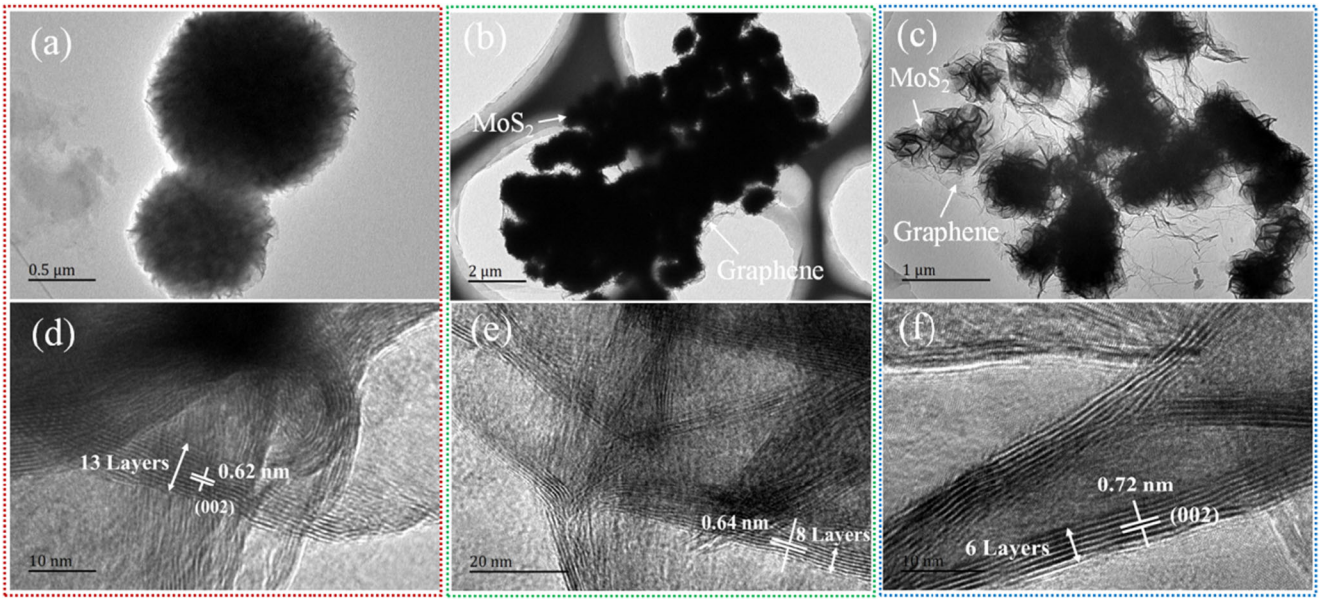


**Fig. 3** TEM (a–c) and HRTEM (d–f) images of the $MoS_2$, $MoS_2$/G, and $MoS_2$/GrF samples, respectively

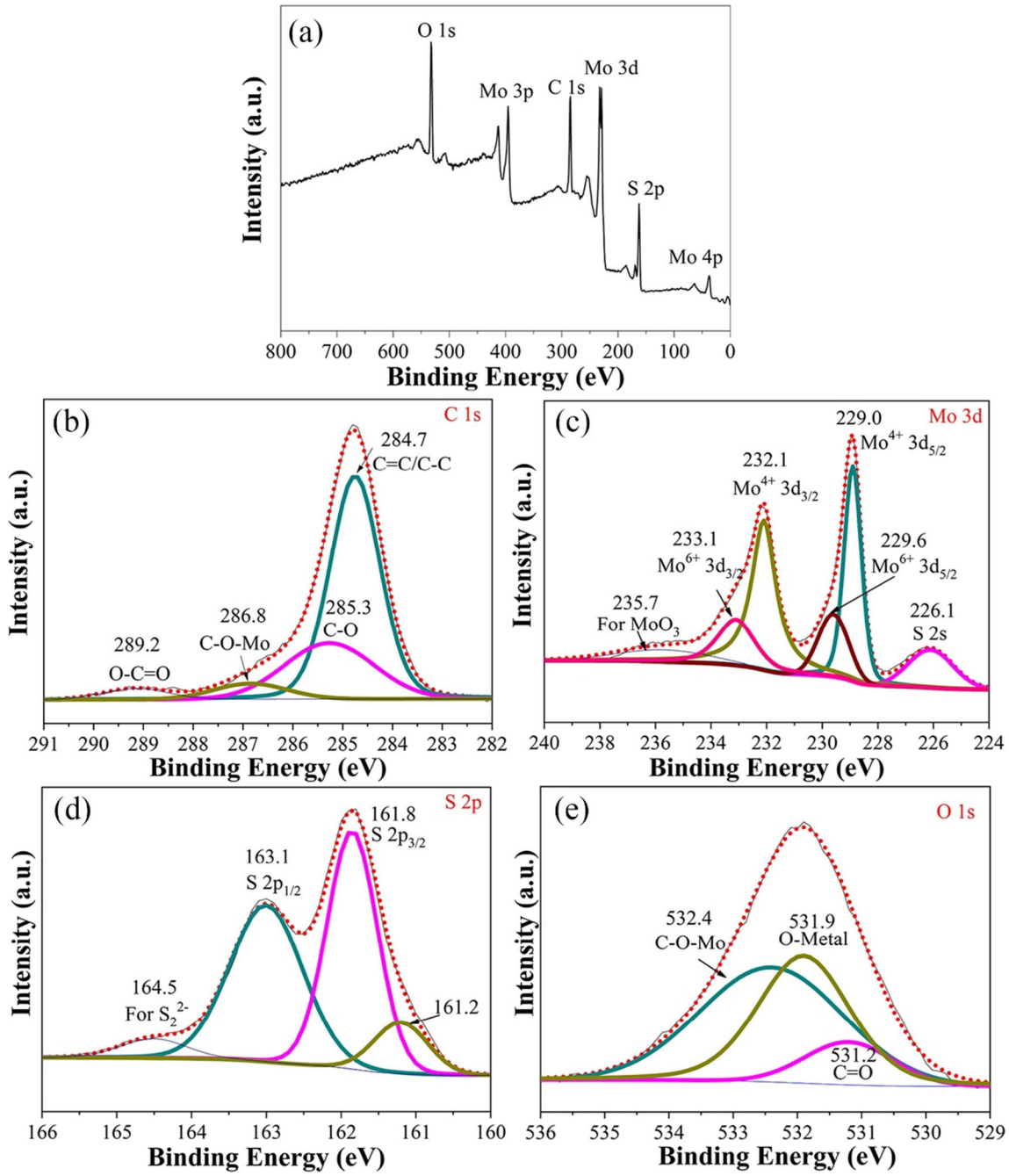


**Fig. 4** a XPS survey spectrum and high-resolution **b** C 1s spectrum, **c** Mo 3d spectrum, **d** S 2p spectrum, and **e** O 1s spectrum of the $MoS_2$/GrF sample

To characterize the nature of the interface between $MoS_2$ and graphene of the $MoS_2$/GrF sample, XPS measurements were carried out. As shown in Fig. 4a, the survey scan spectrum demonstrated the presence of C, Mo, O, and S in the $MoS_2$/GrF sample. Figure 4 b shows the C 1s XPS spectrum of $MoS_2$/GrF, where four different peaks corresponding to C=C/C-C (284.7 eV), C-O (285.3 eV), C-O-Mo (286.8 eV), and O-C=O (289.2 eV) groups were observed [23, 29]. The high-resolution XPS spectrum of the sample in the Mo 3d region is shown in Fig. 4c. It could be deconvoluted into six peaks, and the small peak at 226.1 eV corresponds to the S 2s component of $MoS_2$. The two main intense Mo $3d_{5/2}$ (232.1 eV) and Mo $3d_{3/2}$ (229.0 eV) peaks are characteristic of $Mo^{4+}$ in $MoS_2$ [15, 30], while the peak at 235.7 eV corresponds to $MoO_3$ or $MoO^{2-}$ [31–33]. In addition, the peaks at 233.1 and 229.6 eV are related to the Mo $3d_{5/2}$ and $3d_{3/2}$ components of $Mo^{6+}$, with a spin energy separation of 3.5 eV [30]. The spectrum of S is shown in Fig. 4d. The two major peaks located at 163.1 and 161.8 eV are assigned to the S $2p_{1/2}$ and S $2p_{3/2}$ lines of $MoS_2$, respectively [34]. The peaks of 164.5 eV and

**Table 2** Elemental composition of as-prepared $MoS_2$/GrF synthesized at different reaction times

| Time | Element | | | | | |
|---|---|---|---|---|---|---|
| | C | O | S | Mo | N | S/Mo |
| 2 h | 63.25 | 20.13 | 9.89 | 1.41 | 5.32 | 7.01 |
| 4 h | 60.32 | 18.86 | 13.37 | 3.02 | 4.43 | 4.43 |
| 6 h | 57.68 | 15.77 | 17.10 | 7.02 | 2.43 | 2.43 |
| 8 h | 54.69 | 12.32 | 22.04 | 9.91 | 1.04 | 2.22 |
| 12 h | 44.85 | 9.54 | 29.83 | 15.78 | - | 1.89 |
| 24 h | 44.01 | 8.07 | 31.11 | 16.81 | - | 1.85 |

161.2 eV suggest the existence of bridging $S_2^{2-}$ disulfides and/or apical $S^{2-}$ ligands [35]. Moreover, the oxygen species are shown in Fig. 4e. The three peaks are related to C-O-Mo (532.4 eV), O-metal (531.9 eV), and C=O (531.2 eV) bonds [36–38]. The detection of the C-O-Mo bond proved that a bonding force between $MoS_2$ and graphene in the $MoS_2$/GrF sample existed. Importantly, the C-O-Mo bonds of the $MoS_2$/G composite were verified to provide a good electron transfer path between $MoS_2$ and graphene, which could endow the composite with a highly stable structure for long-term cycling in LIB applications [23].

To better investigate and understand the in situ growth process of $MoS_2$/GrF, the surface morphology of as-prepared $MoS_2$/GrF samples synthesized at different reaction times by the hydrothermal method were determined and are shown in Fig. 5. A few nanoparticles prenucleated on GO are observed in Fig. 5a and b, corresponding to the samples synthesized at reaction times of 2 h and 4 h, respectively. As the reaction time increased, the nanoparticles gradually grew into a flower-like structure, which was distributed uniformly on the substrate. As shown in Fig. 5c, the nucleation of $MoS_x$ gradually increased after 6 h of reaction time. When the reaction time was extended to 8 h, the $MoS_2$ nanoparticles grew uniformly on graphene. As the reaction time was extended to 12 h and 24 h, the surface morphology of the sample did not change much, and flower-like $MoS_2$ nanoparticles grew evenly on graphene. The EDS results can be analyzed by the variation in the S/Mo ratio (Table 2; the samples are pressed into a 5-mm diameter wafer). Clearly, the ratio of S/Mo decreases as the reaction time increases, proving that the $S^{2-}$ ligands can be easily enriched on GO. Finally, the atomic ratio of S and Mo in the sample synthesized at a reaction time of 24 h is 1.85, which is approaching the theoretical value of $MoS_2$. Therefore, we can speculate that the reaction process of as-prepared $MoS_2$/GrF occurred as follows: (1) In the primary reaction period, $S^{2-}$ and $(NH_2)_2^{2-}$ groups reacted preferentially with GO. (2) As the reaction continued, $MoS_x$ crystal nuclei were formed in situ on the GO surface. (3) $H_2S$ is released by $CH_3CSNH_2$ and acts as a S source and reductant simultaneously. Thus, $MoS_2$ nanocrystals could be prepared, and the initial GO sheets were reduced to graphene [39].

Figure 6 a shows the CV performance of $MoS_2$/GrF. The CV measurements were carried out at a scan rate of 0.1 mV $s^{-1}$. Three reduction peaks at 1.5, 1.04, and 0.4 V and two oxidation peaks at 1.82 and 2.35 V are observed during the first cycle. The irreversible reduction peak at 1.5 V can be attributed to the reduction of oxygen-containing functional groups of the graphene; this may be caused by incomplete heat treatment of the sample. The peak at 1.04 V corresponds

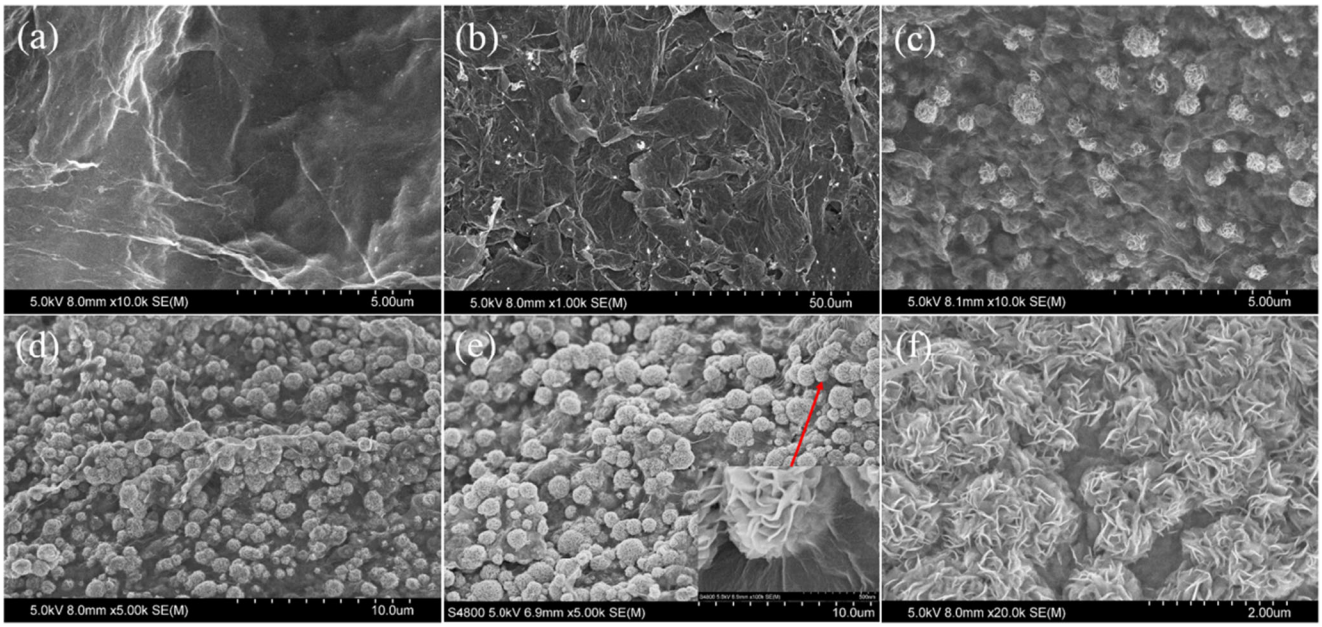


**Fig. 5** FESEM images of as-prepared $MoS_2$/GrF synthesized at different reaction times: a 2 h; b 4 h; c 6 h; d 8 h; e 12 h; and f 24 h

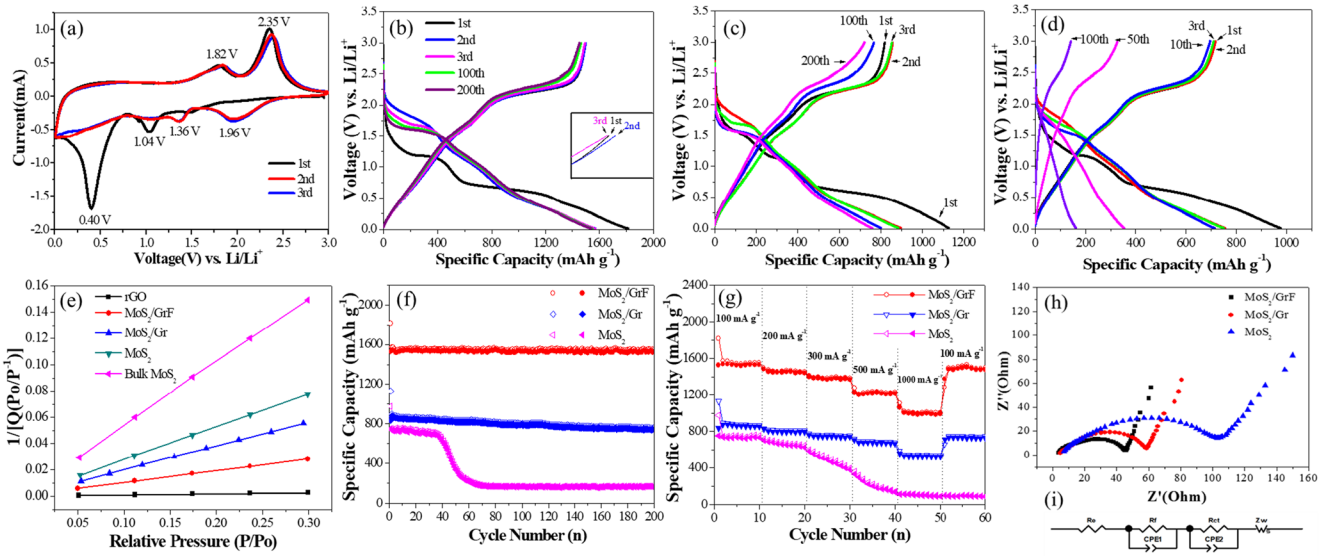


**Fig. 6** Cyclic voltammograms of $MoS_2$/GrF at a scanning rate of 0.1 mV $s^{-1}$ during the first three cycles (**a**). Charge-discharge curves of **b** $MoS_2$/GrF, **c** $MoS_2$/Gr, and **d** $MoS_2$ electrodes at a current density of 100 mA $g^{-1}$. BET surface area plot of electrodes (**e**). Cycling performance of $MoS_2$/GrF, $MoS_2$/Gr, and $MoS_2$ electrodes at a current density of 100 mA $g^{-1}$ for 200 cycles (**f**). Rate performances of $MoS_2$, $MoS_2$/Gr, and $MoS_2$/GrF composite electrodes at different current densities (**g**). Nyquist plots of $MoS_2$, $MoS_2$/Gr, and $MoS_2$/GrF electrodes in the frequency range from 200 kHz to 0.01 Hz (**h**) and the equivalent-circuit model (**i**)

to $Li^+$ intercalation into the $MoS_2$ interlayer space and subsequent formation of $Li_xMoS_2$, which is accompanied by a phase transformation from the 2H to the 1T structure of $Li_xMoS_2$ ($MoS_2 + xLi^+ + xe^- \rightarrow Li_xMoS_2$) [17, 21, 40]. The peak at 0.4 V can be ascribed to the conversion of $Li_xMoS_2$ into $Li_2S$ and metallic Mo ($Li_xMoS_2 + (4\text{-}x)e^- \rightarrow Mo + 2Li_2S$) [14, 41, 42]. The oxidation peaks at 2.35 and 1.82 V were ascribed to the partial oxidation of Mo at 2.35 V ($Mo + xLi_2S \rightarrow MoS_2$) [27] and the restacked $MoS_2$ with an enlarged interlayer distance, respectively [43]. In the 2nd and 3rd cycles of the cathode sweep, the peaks located at 1.5, 1.04, and 0.4 V disappear, and two reduction peaks at 1.96 V and 1.36 V could be observed, which agrees with the previous lithiation and delithiation profiles. [44] Moreover, except for the first discharge curve, each curve is almost identical, suggesting that the $MoS_2$/GrF electrode has excellent stability during the electrochemical processes.

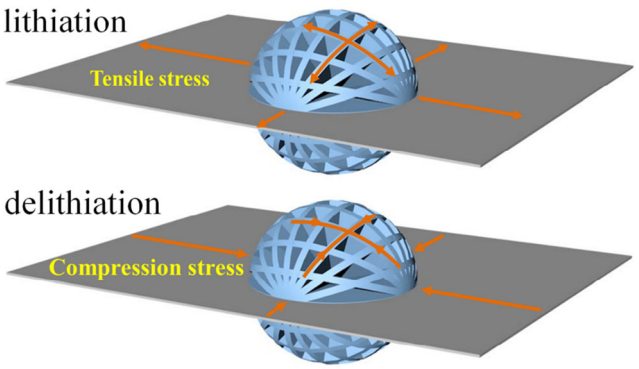


**Scheme 1** The mechanical model of the $MoS_2$/GrF electrode during the lithiation and delithiation processes

The discharge-charge profiles of the $MoS_2$/GrF electrode for the 1st, 2nd, 3rd, 100th, and 200th cycles at a current density of 100 mA $g^{-1}$ between 3.0 and 0.01 V are shown in Fig. 6b. The $MoS_2$/GrF electrode exhibited an excellent initial discharge/charge capacity of 1528/1814 mAh $g^{-1}$ with a coulombic efficiency of approximately 84.2%. Obviously, the irreversible capacity loss during the first cycle can be attributed to the formation of a solid-electrolyte interphase (SEI) layer [21, 45]. Moreover, the efficiency was maintained at nearly 99% in the subsequent cycles. By contrast, Fig. 6c and d present the discharge-charge performance of $MoS_2$/Gr and $MoS_2$. The first discharge/charge capacities of $MoS_2$/Gr and $MoS_2$ were 835/1130 mAh $g^{-1}$ and 748/977 mAh $g^{-1}$, with initial coulombic efficiencies of 73.9% and 76.5%, respectively. To identify the factors influencing the high capacity of Mo/GrF, a specific surface area (BET) test was performed. As shown in Fig. 6e, the BET surface area of $MoS_2$/GrF was higher than those of $MoS_2$/GrF and $MoS_2$, proving that the $MoS_2$/GrF sample had more active sites for lithium ions. The synergetic effect between graphene and $MoS_2$ also greatly enhanced the lithium storage capacity of $MoS_2$/GrF [23].

The cycling performance of the $MoS_2$/GrF electrode was evaluated and is presented in Fig. 6f. For comparison, the respective performance data for the $MoS_2$/Gr and $MoS_2$ electrodes are also included. After 39 cycles, the capacity of the $MoS_2$ electrode showed a marked decrease to approximately 165 mAh $g^{-1}$. The damage of the structure by volume changes likely led to the pulverization of the active material [23]. The capacity of the $MoS_2$/Gr electrode exhibited a slow decrease from 1130 to 758 mAh $g^{-1}$ after 200 cycles. Interestingly, the $MoS_2$/GrF electrode delivered a stable and reversible capacity

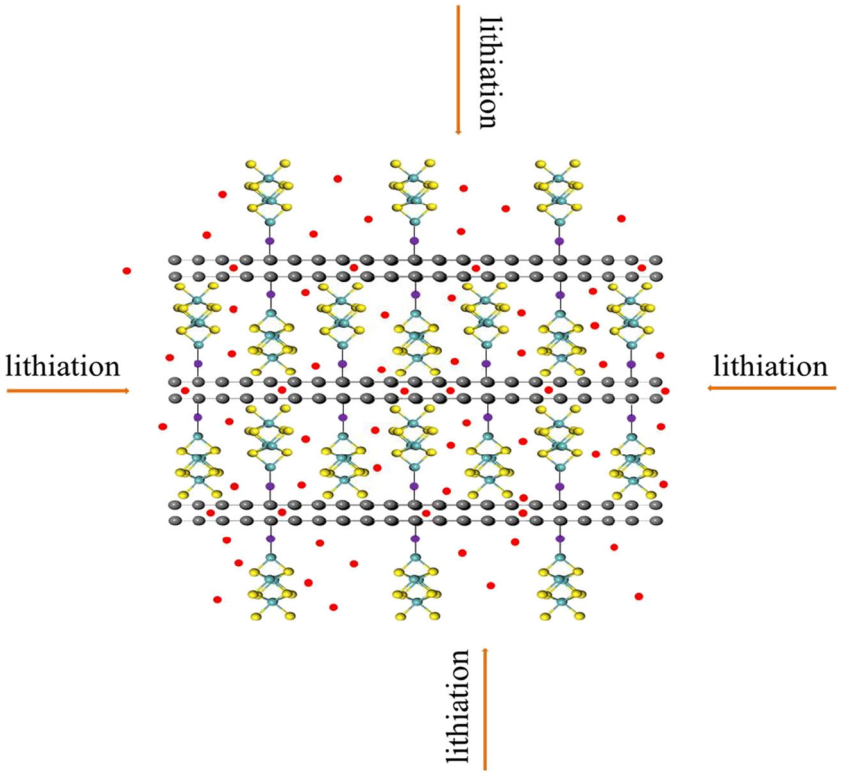


**Scheme 2** The diffusion path of lithium ions in the $MoS_2$/GrF electrode

of 1510 mAh $g^{-1}$ after 200 cycles. Comparing the three electrodes demonstrated that the unique three-dimensional hierarchical structure of $MoS_2$/GrF can greatly improve its cycling stability. As illustrated in Scheme 1, the flower-like $MoS_2$ on the $MoS_2$/GrF sample had a network-like architecture, which had good structural stability. When $MoS_2$/GrF was used as an electrode material, the network-like architecture could resist the expansion and shrinkage during the lithiation and delithiation processes. Furthermore, graphene acts as a buffer base, which could be helpful for the resistance against structural deformation.

To evaluate the rate cycling behavior of the three electrodes, tests were carried out at different current densities, as shown in Fig. 6g. For the $MoS_2$/GrF electrode, the 10th cycle discharge capacities were approximately 1550, 1450, 1380, 1220, and 990 mAh $g^{-1}$ at current densities of 100, 200, 300, 500, and 1000 mA $g^{-1}$, respectively. When the current density changed from 1000 to 100 mA $g^{-1}$, the discharge capacity of the electrode returned to ~1500 mAh $g^{-1}$, indicating the extraordinarily high cycling stability of the $MoS_2$/GrF sample. For comparison, $MoS_2$/Gr and $MoS_2$ electrodes were evaluated at the same current density. The $MoS_2$/Gr electrode exhibited a discharge capacity of approximately 530 mAh $g^{-1}$ at a current density of 1000 mA $g^{-1}$, and the discharge capacity was approximately 740 mA $g^{-1}$ when the current density returned to 100 mA $g^{-1}$. In the case of $MoS_2$, the discharge capacity was 750 mAh $g^{-1}$ at a current density of 100 mA $g^{-1}$. However, the capacity of the $MoS_2$ electrode showed a rapid decline to 100 mAh $g^{-1}$ at a current density of 1000 mA $g^{-1}$, and the capacity was not reversible when the current density was restored to 100 mA $g^{-1}$. According to relevant studies [23], the outstanding rate performance of the $MoS_2$/GrF composite can be ascribed to the C-O-Mo bonds between $MoS_2$ and graphene. In addition, the HRTEM results reveal that the $MoS_2$/GrF composite exhibited a larger (002) interlayer distance than the $MoS_2$/Gr and $MoS_2$ samples. This provided a larger space for $Li^+$ intercalation, thereby facilitating faster Li-ion diffusion [27].

To better understand the superior electrochemical performance of the samples, alternating-current impedance measurements were performed after 10 cycles, as shown in Fig. 6h, and the equivalent-circuit model is shown in Fig. 6i. According to a previous report, $R_e$ denotes the internal resistance of the battery. The high-frequency semicircle in Fig. 10a could be attributed to resistance $R_f$ and $CPE_1$ of the SEI film. The medium-frequency semicircle is assigned to the charge-transfer resistance $R_{ct}$ and $CPE_2$ of the electrode/electrolyte interface. The inclined line in the low-frequency region belongs to $Z_w$, which is considered the Warburg impedance corresponding to the lithium-diffusion process. According to the equivalent-circuit model in Fig. 6i, the $R_f$ and $R_{ct}$ of the $MoS_2$/GrF electrode are 9.58 Ω and 38.72 Ω, respectively, which are less than those of $MoS_2$/Gr ($R_f$=12.53 Ω and $R_{ct}$=51.62 Ω) and $MoS_2$ ($R_f$=17.25 Ω and $R_{ct}$=123.1 Ω). In particular, the $R_{ct}$ of $MoS_2$/GrF is only 75% and 31% of those of the $MoS_2$/Gr and $MoS_2$ electrodes, respectively. This finding implies a

reduction in contact resistance and charge-transfer resistance during $Li^+$ insertion/extraction reactions of the $MoS_2$/GrF electrode due to its unique three-dimensional hierarchical heterogeneous structure. This result was similar to that reported by Shan et al.,[16] who considered that the unique hierarchical 3F top-down architecture not only helped accommodate the volume variation during the cycling process but also diminished the excess interface between the electrode and electrolyte.

## Conclusions

A facile process for synthesizing a unique three-dimensional hierarchical heterogeneous structure of $MoS_2$/GrF by the hydrothermal method and a subsequent annealing process performed under a $N_2$ atmosphere at 800 °C for 2 h was developed. The outstanding electrochemical performance of $MoS_2$/GrF can be attributed to its designed structure. As illustrated in Scheme 2, the advantages of the three-dimensional structure of the $MoS_2$/GrF electrode are manifested in three aspects. First, the flower-like $MoS_2$ microspheres are grown in situ on graphene, and the $MoS_2$ microspheres consist of approximately 5-nm thick nanosheets, which can provide abundant active edge sites for reactions with lithium. In addition, due to the hierarchical heterostructure, there is no stacking of graphene, promoting good contact between the active sites of graphene and the electrolyte. Thus, the synergistic effect of $MoS_2$ and graphene led to a high lithium storage capacity. Second, the C-O-Mo bond acts as an internal contact, and the layer contact acts as an external contact. This special structure could provide a good electron transfer path between $MoS_2$ and graphene and endow the composite with excellent rate performance [26]. The larger lattice plane spacing corresponding to the (002) plane of $MoS_2$/GrF not only provided more space for Li-ion intercalation but also led to faster Li-ion diffusion. Third, the network-like architecture of $MoS_2$ could enhance the architecture stability and resist volume expansion during lithiation and delithiation processes. Meanwhile, graphene acts as a buffer to resist volume expansion. Therefore, the structure is stable toward long-term cycling in LIB applications. The unique three-dimensional hierarchical heterogeneous structure of the $MoS_2$/GrF composite can be considered a promising anode material candidate for high-performance LIBs.

**Supplementary Information** The online version contains supplementary material available at https://doi.org/10.1007/s11581-021-03936-y.

**Funding** We acknowledge the financial support from the National Natural Science Foundation of China (No.51972071), Guangxi Distinguished Experts Special Fund (No.2019B06), and Guangxi Research Foundation for Science and Technology Base and Talent Special (No.AD19245175) and Opening Fund of Guangxi Key Laboratory of Building New Energy and Energy Saving (No.18-J-21-6).

## References

1. Li Y, Jiang S, Qian Y, Yan X, Zhou J, Yi Z, Lin N, Qian Y (2020) 2D interspace confined growth of ultrathin $MoS_2$-intercalated graphite hetero-layers for high-rate Li/K storage. Nano Res 14: 1061–1068
2. Qin M, Ren W, Meng J, Wang X, Mai L (2019) Realizing superior prussian blue positive electrode for potassium storage via ultrathin nanosheet assembly. ACS Sustain Chem Eng 13:11564–11570
3. Ren W, Qin M, Zhu Z, Yan M, Li Q, Zhang L, Liu D, Mai L (2017) Activation of sodium storage sites in prussian blue analogues via surface etching. Nano Lett 8:4713–4718
4. Li JH, Tao HC, Zhang YK, Yang XL (2019) Molybdenum disulfide/reduced graphene oxide nanocomposite with expanded interlayer spacing for sodium ion batteries. J Electrochem Soc 15: A3685–A3692
5. Zhang YQ, Tao HC, Li T, Du SL, Li JH, Zhang YK, Yang XL (2018) Vertically oxygen-incorporated $MoS_2$ nanosheets coated on carbon fibers for sodium-ion batteries. ACS Appl Mater Interfaces 10:35206–35215
6. Chang K, Chen W, Ma L, Li H, Li H, Huang F, Xu Z, Zhang Q, Lee JY (2011) Graphene-like $MoS_2$/amorphous carbon composites with high capacity and excellent stability as anode materials for lithium ion batteries. J Mater Chem 17:6251–6257
7. Stephenson T, Li Z, Olsen B, Mitlin D (2014) Lithium ion battery applications of molybdenum disulfide ($MoS_2$) nanocomposites. Energy Environ Sci 1:209–231
8. Tian R, Wang W, Huang Y, Duan H, Guo Y, Kang H, Li H, Liu H (2016) 3D composites of layered $MoS_2$ and graphene nanoribbons for high performance lithium-ion battery anodes. J Mater Chem A 34:13148–13154
9. Zhang R, Tang Z, Wang HY, Sun D, Tang YG, Xie ZY (2020) The fabrication of hierarchical $MoO_2$@$MoS_2$/rGO composite as high reversible anode material for lithium ion batteries. Electrochim Acta 364:136996
10. Choi JH, Kim MC, Moon SH, Kim H, Kim YS, Park KW (2020) Enhanced electrochemical performance of MoS2/graphene nanosheet nanocomposites. RSC Adv 32:19077–19082
11. Wang C, Wan W, Huang Y, Chen J, Zhou HH, Zhang XX (2014) Hierarchical $MoS_2$ nanosheet/active carbon fiber cloth as a binder-free and free-standing anode for lithium-ion batteries. Nanoscale 10:5351–5358
12. Wan Z, Shao J, Yun J, Zheng H, Gao T, Shen M, Qu Q, Zheng H (2014) Core-shell structure of hierarchical quasi-hollow $MoS_2$ microspheres encapsulated porous carbon as stable anode for Li-ion batteries. Small 23:4975–4981
13. Zhang L, Lou XW (2014) Hierarchical $MoS_2$ shells supported on carbon spheres for highly reversible lithium storage. Chemistry 18: 5219–5223
14. Ding S, Chen JS, Lou XW (2011) Glucose-assisted growth of $MoS_2$ nanosheets on CNT backbone for improved lithium storage properties. Chemistry 47:13142–13145
15. Wang S, Jiang X, Zheng H, Wu H, Kim SJ, Feng C (2012) Solvothermal synthesis of $MoS_2$/carbon nanotube composites with improved electrochemical performance for lithium ion batteries. Nano Nanotechnol Lett 4:378–383

16. Chang K, Chen WX (2011) L-cysteine-assisted synthesis of layered $MoS_2$/graphene composites with excellent electrochemical performances for lithium ion batteries. ACS Nano 6:4720–4728
17. Liu Y, Zhao Y, Jiao L, Chen J (2014) A graphene-like $MoS_2$/graphene nanocomposite as a highperformance anode for lithium ion batteries. J Mater Chem A 32:13109–13115
18. Zhou X, Wan LJ, Guo YG (2013) Synthesis of $MoS_2$ nanosheet-graphene nanosheet hybrid materials for stable lithium storage. Chem Commun (Camb) 18:1838–1840
19. Zhang YQ, Tao HC, Ma H, Du SL, Li T, Zhang YK, Li JH, Yang XL (2018) Three-dimensional $MoO_2$@few-layered $MoS_2$ covered by S-doped graphene aerogel for enhanced lithium ion storage. Electrochim Acta 283:619–627
20. Gong YJ, Yang SB, Zhan L, Ma LL, Vajtai R, Ajayan PM (2014) A bottom-up approach to build 3D architectures from nanosheets for superior lithium storage. Adv Funct Mater 1:125–130
21. Wang J, Liu J, Chao D, Yan J, Lin J, Shen ZX (2014) Self-assembly of honeycomb-like $MoS_2$ nanoarchitectures anchored into graphene foam for enhanced lithium-ion storage. Adv Mater 42:7162–7169
22. Pan F, Wang J, Yang Z, Gu L, Yu Y (2015) $MoS_2$–graphene nanosheet–CNT hybrids with excellent electrochemical performances for lithium-ion batteries. RSC Adv 95:77518–77526
23. Teng Y, Zhao H, Zhang Z, Li Z, Xia Q, Zhang Y, Zhao L, Du X, Du Z, Lv P, Swierczek K (2016) $MoS_2$ nanosheets vertically grown on graphene sheets for lithium-ion battery anodes. ACS Nano 9:8526–8535
24. Shan TT, Xin S, You Y, Cong HP, Yu SH, Manthiram A (2016) Combining nitrogen-doped graphene sheets and $MoS_2$: a unique film-foam-film structure for enhanced lithium storage. Angew Chem Int Ed Eng 41:12783–12788
25. Hummers WS, Offeman RE (1958) Preparation of graphitic oxide. J Am Chem Soc 6:1339–1339
26. Chen S, Chen P, Wu M, Pan D, Wang Y (2010) Graphene supported Sn–Sb@carbon core-shell particles as a superior anode for lithium ion batteries. Electrochem Commun 10:1302–1306
27. Hwang H, Kim H, Cho J (2011) $MoS_2$ nanoplates consisting of disordered graphene-like layers for high rate lithium battery anode materials. Nano Lett 11:4826–4830
28. Xie KY, Yuan K, Li X, Lu W, Shen C, Liang CL, Vajtai R, Ajayan P, Wei BQ (2017) Superior potassium ion storage via vertical $MoS_2$ "nano-rose" with expanded interlayers on graphene. Small 42:1–8
29. Zhou JS, Li JM, Liu KH, Lan L, Song HH, Chen XH (2014) Free-standing cobalt hydroxide nanoplatelet array formed by growth of preferential-orientation on graphene nanosheets as anode material for lithium-ion batteries. J Mater Chem A 48:20706–20713
30. Sun Y, Hu X, Luo WHuang Y (2012) Ultrafine $MoO_2$ nanoparticles embedded in a carbon matrix as a high-capacity and long-life anode for lithium-ion batteries. J Mater Chem 2:425–431
31. Koroteev VO, Bulusheva LG, Asanov IP, Shlyakhova EV, Vyalikh DV, Okotrub AV (2011) Charge transfer in the $MoS_2$/carbon nanotube composite. J Phys Chem C 43:21199–21204
32. Wang HW, Skeldon P, Thompson GE (1997) XPS studies of $MoS_2$ formation from ammonium tetrathiomolybdate solutions. Surf Coat Technol 3:200–207
33. Sun YM, Hu XL, Yu JC, Li Q, Luo W, Yuan LX, Zhang WX, Huang YH (2011) Morphosynthesis of a hierarchical $MoO_2$ nanoarchitecture as a binder-free anode for lithium-ion batteries. Energy Environ Sci 4:2870–2877
34. Zheng XL, Xu JB, Yan KY, Wang H, Wang ZL, Yang SH (2014) Space-confined growth of $MoS_2$ nanosheets within graphite: the layered hybrid of $MoS_2$ and graphene as an active catalyst for hydrogen evolution reaction. Chem Mater 7:2344–2353
35. Vrubel H, Merki D, Hu X (2012) Hydrogen evolution catalyzed by $MoS_3$ and $MoS_2$ particles. Energy Environ Sci 5:6136–6144
36. Li L, Zhou GM, Weng Z, Shan XY, Li F, Cheng HM (2014) Monolithic $Fe_2O_3$/graphene hybrid for highly efficient lithium storage and arsenic removal. Carbon 67:500–507
37. Zhou GM, Wang DW, Yin LC, Li N, Li F, Cheng HM (2012) Oxygen bridges between NiO nanosheets and graphene for improvement of lithium storage. ACS Nano 4:3214–3223
38. Xu HP, Shi LY, Wang ZY, Liu J, Zhu JF, Zhao Y, Zhang MH, Yuan S (2015) Fluorine-doped tin oxide nanocrystal/reduced graphene oxide composites as lithium ion battery anode material with high capacity and cycling stability. ACS Appl Mater Interfaces 49:27486–27493
39. Zhang SP, Chowdari BVR, Wen ZY, Jin J, Yang JH (2015) Constructing highly oriented configuration by few-layer $MoS_2$: toward high-performance lithium-ion batteries and hydrogen evolution reactions. ACS Nano 12:12464–12472
40. Tang YP, Wu DQ, Mai YY, Pan H, Cao J, Yang CQ, Zhang F, Feng XL (2014) A two-dimensional hybrid with molybdenum disulfide nanocrystals strongly coupled on nitrogen-enriched graphene via mild temperature pyrolysis for high performance lithium storage. Nanoscale 24:14679–14685
41. Fang XP, Yu XQ, Liao SF, Shi YF, Hu YS, Wang ZX, Stucky GD, Chen LQ (2012) Lithium storage performance in ordered mesoporous $MoS_2$ electrode material. Microporous Mesoporous Mater 151:418–423
42. Ding S, Zhang D, Chen JS, Lou XW (2012) Facile synthesis of hierarchical $MoS_2$ microspheres composed of few-layered nanosheets and their lithium storage properties. Nanoscale 1:95–98
43. Du G, Guo Z, Wang S, Zeng R, Chen Z, Liu H (2010) Superior stability and high capacity of restacked molybdenum disulfide as anode material for lithium ion batteries. Chem Commun (Camb) 7:1106–1108
44. Wang Z, Chen T, Chen WX, Chang K, Ma L, Huang GC, Chen DY, Lee JY (2013) CTAB-assisted synthesis of single-layer $MoS_2$-graphene composites as anode materials of Li-ion batteries. J Mater Chem A 6:2202–2210
45. Sheng JZ, Wang TS, Tan JY, Lv W, Qiu L, Zhang QF, Zhou GM, Cheng HM (2020) Intercalation-induced conversion reactions give high-capacity potassium storage. ACS Nano 10:14026–14035

**Publisher's note** Springer Nature remains neutral with regard to jurisdictional claims in published maps and institutional affiliations.